HHS Public Access

Author manuscript

Clin Cancer Res. Author manuscript; available in PMC 2019 April 01.

Published in final edited form as:

Clin Cancer Res. 2018 April 01; 24(7): 1574–1585. doi:10.1158/1078-0432.CCR-17-2057.

Thy1-Targeted Microbubbles for Ultrasound Molecular Imaging of Pancreatic Ductal Adenocarcinoma

Lotfi Abou-Elkacem[1], **Huaijun Wang**[1], **Sayan M. Chowdhury**[1], **Richard H. Kimura**[1], **Sunitha V. Bachawal**[1], **Sanjiv S. Gambhir**[1], **Lu Tian**[2], and **Jürgen K. Willmann**[1,*]

[1]Department of Radiology, Molecular Imaging Program at Stanford, California, USA

[2]Department of Health, Research & Policy, Stanford University, Stanford, California, USA

Abstract

Purpose—To engineer a dual human and murine Thy1-binding single-chain-antibody ligand (Thy1-scFv) for contrast microbubble-enhanced ultrasound molecular imaging of pancreatic ductal adenocarcinoma (PDAC).

Experimental Design—Thy1-scFv were engineered using yeast-surface-display techniques. Binding to soluble human and murine Thy1 and to Thy1-expressing cells was assessed by flow cytometry. Thy1-scFv was then attached to gas-filled microbubbles to create $MB_{Thy1\text{-}scFv}$. Thy1 binding of $MB_{Thy1\text{-}scFv}$ to Thy1-expressing cells was evaluated under flow shear stress conditions in flow-chamber experiments. $MB_{scFv\text{-}scrambled}$ and $MB_{Non\text{-}targeted}$ were used as negative controls. All microbubble types were tested in both orthotopic human PDAC xenografts and transgenic PDAC mice *in vivo*.

Results—Thy1-scFv had a K_D of 3.4±0.36 nM for human and 9.2±1.7 nM for murine Thy1 and showed binding to both soluble and cellularly expressed Thy1. $MB_{Thy1\text{-}scFv}$ attached to Thy1 with high affinity compared to negative control microbubbles (P<0.01) as assessed by flow cytometry. Similarly, flow-chamber studies showed significantly (P<0.01) higher binding of $MB_{Thy1\text{-}scFv}$ (3.0±0.81 MB/cell) to Thy1-expressing cells than $MB_{scFv\text{-}scrambled}$ (0.57±0.53) and $MB_{Non\text{-}targeted}$ (0.43±0.53). *In vivo* ultrasound molecular imaging using $MB_{Thy1\text{-}scFv}$ demonstrated significantly higher signal (P<0.01) in both orthotopic (5.32±1.59 a.u.) and transgenic PDAC (5.68±2.5 a.u.) mice compared to chronic pancreatitis (0.84±0.6 a.u.) and normal pancreas (0.67±0.71 a.u.). *Ex vivo* immunofluorescence confirmed significantly (P<0.01) increased Thy1 expression in PDAC compared to chronic pancreatitis and normal pancreas tissue.

Conclusions—A dual human and murine Thy1-binding scFv was designed to generate contrast microbubbles to allow PDAC detection with ultrasound.

Keywords

Pancreatic ductal adenocarcinoma; single-chain antibody; ultrasound; molecular imaging; microbubbles

*Corresponding author: Jürgen K. Willmann, M.D., Department of Radiology, School of Medicine, Stanford University, 300 Pasteur Drive, Room H1307, Stanford, CA 94305-5621. P: 650-723-5424; Fax: 650-723-1909; willmann@stanford.edu.

Conflict of interest statement: The authors declare no conflicts of interest.

Introduction

Pancreatic ductal adenocarcinoma (PDAC) is a highly lethal form of cancer and is currently the fourth leading cause of cancer death in the USA (1). The American Cancer Society estimated 53,670 new diagnoses of PDAC and 43,090 deaths from this cancer in 2017 in the USA (1). The incidence of PDAC is on the rise and PDAC is projected to become the second most common cause of cancer death in the USA by 2030 (2). While patient survival is highly dependent upon tumor stage, most patients already have advanced disease at the time of diagnosis (3). Therefore, the overall median survival of patients after diagnosis is only 4 to 6 months (4). While unpredictable and vague clinical symptoms related to the disease are factors in the delay in diagnosis, there is a lack of specific and sensitive blood biomarker or imaging tests to detect the disease early (5).

One potential strategy for earlier detection of PDAC involves the screening of moderate and high-risk patients using molecularly-targeted contrast microbubbles that bind and amplify the signal of molecular markers differentially expressed on the neovasculature of PDAC compared with normal pancreas and chronic pancreatitis (6–8). Proteomic analysis and immunohistochemical staining of whole tissues from human PDAC and control normal pancreas and chronic pancreatitis have previously identified and validated the thymocyte differentiation antigen 1 (Thy1) as a molecular marker differentially upregulated on the neovasculature of PDAC (6,9). 81% of PDAC cases stained positive for Thy1 while normal pancreas and chronic pancreatitis cases were positive in 11% and 7%, respectively. Thy1 neovascular immunostaining could distinguish PDAC from normal and chronic pancreatitis tissues with 90% specificity and 81% sensitivity. Thy1, also known as cluster of differentiation 90 or CD90, is a cell-surface glycoprotein that belongs to the immunoglobulin-like supergene family. Thy1 was originally described as a mouse thymocyte differentiation marker (10,11) and subsequently shown to be expressed in other tissues, including the surface of newly formed blood vessels in human colon cancer (12), glioblastoma (13), hepatocellular carcinoma (14), and ovarian cancer tissues (15).

Evolving protein display techniques (16) using naïve nonimmune human single chain fragment variable (scFv) yeast surface display (YSD) libraries enable the development of novel ligands with high affinity, specificity, and stability that can be used to functionalize contrast microbubbles to attach to molecular markers. An antibody in scFv format (molecular weight of ~28 kDa) consists of variable regions of heavy (VH) and light (VL) chains, joined together by a flexible peptide linker (17). ScFvs are an alternative to full-length antibodies in diagnostic and therapeutic applications and have been translated to clinical trials (18–20). In comparison to full-length antibodies, scFv have shown to be advantageous for molecular imaging due to better tumor penetration, more rapid blood clearance, shorter retention times in non-target tissues, as well as reduced immunogenicity (21–23). Furthermore, due to their relatively small size as well as good stability and solubility, scFvs can be recombinantly produced in a cost efficient way (24,25). Moreover, the high stability of scFvs with a single lysine distant from the paratope/antigen-binding site ease amine bioconjugation chemistry to functionalize contrast microbubbles (26).

The purpose of this proof-of-principle study was to engineer a human scFv ligand binding to both human and murine Thy1 and to test it for *in vivo* ultrasound molecular imaging in two different mouse models of PDAC, in human xenografts and transgenic PDAC mice.

Materials and Methods

Human Thy1-Expressing Vascular Endothelial Cells

Wildtype MILE SVEN 1 mouse vascular endothelial (MS1-WT) cells were obtained directly obtained directly from American Type Culture Collection [(CRL2279; (ATCC)] that performs standard cell line characterizations of mycoplasma, yeast, bacterial and viral contamination. The cell line was maintained according to the recommendations of the ATCC. Cells were cultured under sterile conditions in Dulbecco's Modified Eagle Medium (ATCC) with FBS at 5% and maintained in a 5% CO2-humidified atmosphere at 37°C. Cells were transfected with human Thy1 DNA as described (6). In brief, the human Thy1 DNA sequence (gi|224589802:c119294246-119288655) was first optimized for mammalian codon usage using standard techniques (27). The transfection of MS1-WT cells with the Thy1-expression vector was performed using lipofectamine 2000 transfection reagent (Life Sciences; Invitrogen), following the recommended manufacturer's standard protocol. MS1 cells stably expressing human Thy1 ($MS1_{Thy1}$) were grown in DMEM containing 10% fetal bovine serum and 0.4 mg/ml puromycin (G418, Sigma, St. Louis, MO) in a 5% CO_2 humidified atmosphere and subcultured prior to confluence using trypsin.

Engineering of an Thy1-targeted single-chain antibody (Thy1-scFv)

A yeast surface displayed nonimmune human scFv library was sorted and matured as described (16). For further details, please refer to Supplementary Methods.

Affinity measurements of Thy1-scFv against human and murine Thy1

The dissociation constant (K_D) of the Thy1-scFv were measured using yeast as described (28). In brief, yeast cells (1×10^5) transformed with pCT plasmid containing Thy1-scFv gene were incubated with 0.01 to 100 nM recombinant human and murine biotinylated Fc-conjugated Thy1 (B-Thy1, Abcam), respectively, overnight at room temperature. Cells were stained with the chicken anti-c-myc antibody (eBioscience). After FACS analysis, mean fluorescence values for streptavidin-allophycocyanin (APC; Biolegend) and Alexa 555-conjugated goat anti-chicken IgY (eBioscience) in double-positive populations of each yeast sample were acquired. K_D values were analyzed by determining the ratio of the mean fluorescence intensity of [APC] and fluorescence intensity of [A555] using FACS. The ratio was plotted against the used concentration of Thy1 using Prism 5 software (Graphpad, CA). The K_D was determined using a nonlinear least squares curve fit (16,29,30).

Purification of Thy1-scFv

Thy1-scFv ligand was recombinantly expressed in SHuffle T7 Escherichia coli and purified by a HisTrap FF column (GE Healthcare Biosciences, PA). For further details, please refer to Supplementary Methods.

In vitro binding analysis of purified Thy1-scFv

Thy1-coated magnetic beads were prepared as described above, and analyzed with FACS. Briefly, 66 pmol of Fc-conjugated human and murine Thy1 was incubated with 10 μL of protein G-magnetic beads (ThermoFisher Scientific) in 50 μL of PBSA for 40 min at room temperature. As controls, naked protein G-beads and beads coated with the same amount of human and murine IgG were prepared. Subsequently, beads were washed with PBSA and incubated with 10nM purified biotinylated Thy1-scFv for 1.5 hours at room temperature. The Thy1-scFv bound to beads were stained with 5 μL of streptavidin-APC (Biolegend) and analyzed by FACS. For cell binding assay, $MS1_{Thy1}$ was stained with APC-labeled Thy1-scFv for 1.5 hours at 4°C and analyzed with FACS. As negative control cells, both MS1-WT and $MS1_{CD276}$, a cell line overexpressing an independent biomarker CD276, were stained with Thy1-scFv. To confirm Thy1 expression on cells, primary antibody (rabbit anti-human Thy1, Sigma, 1:100) incubation was performed. After washing in PBS, secondary antibody (anti-rabbit FITC, Jackson Immunolaboratories, 1:500) was added for one hour at 4°C and analyzed with FACS.

In vitro immunofluorescence staining of human Thy1-expressing murine vascular endothelial cells

To confirm human Thy1 expression on vascular endothelial MS1 cells, immunofluorescence staining of the cells was performed using standard techniques. In brief, MS1-WT and $MS1_{Thy1}$ cells were grown on cover slips under standard conditions in DMEM complete growth media for 24 hours; after the media was removed, cells were washed in PBS and fixed in 4% paraformaldehyde in PBS solution for 30 min at room temperature. Cells were then washed in PBS, and 1% bovine serum albumin (BSA) blocking solution was applied for one hour. The biotinylated Thy1-scFv (100nM) incubation was performed for 2h at 4°C. After washing in PBS, secondary antibody (Streptavidin-AF555, ThermoFisher Scientific) was added for one hour at room temperature. Cells were then washed in PBS, counterstained with 4′,6 diamidino-2-phenylindole (DAPI), mounted onto glass slides with anti-fade solution and imaged with an Olympus IX81 system.

Preparation of Thy1-targeted microbubbles

Commercially available perfluorocarbon-filled, lipid-shelled, streptavidin-coated microbubbles (MicroMarker, VisualSonics, Toronto, Canada) were used to generate Thy1-targeted microbubbles. Microbubbles targeted to both human and murine Thy1 ($MB_{Thy1\text{-}scFv}$) using the new Thy1-scFv. Two positive control microbubbles (MB_{Thy1}) targeted either to murine Thy1 (for imaging of transgenic mice) or to human Thy1 (for human xenograft imaging) using commercially available antibodies as binding ligands. $MB_{scFv\text{-}scrambled}$ and $MB_{Non\text{-}targeted}$ were used as negative controls. For further details, please refer to Supplementary Methods.

Assessment of scFv conjugation on microbubble surface

Successful coupling of both Thy1-scFv and $scFv_{scrambled}$ on the microbubble shell was confirmed by FACS and microscopy. Synthesized targeted microbubbles (1×10^5 each) coupled with either Thy1-scFv and $scFv_{Scrambled}$ were incubated with an anti-His antibody-

AF488 (Thermo Fisher, USA) for 1h. The labeled molecularly-targeted microbubbles were washed three times by centrifugation at 300g for 2 min and analyzed by FACS. FACS was used to confirm microbubble ligand coating by fluorescence intensity. Voltage, forward and side light scattering (FSC and SSC) settings were adjusted to detect solely microbubble populations. 50 μL freshly synthesized microbubble solutions were diluted with 200 μL PBS prior to each measurement. Subsequent data analysis was done using FlowJo software (Stanford University, CA, USA).

In vitro flow cytometry Thy1-binding studies of scFv-conjugated microbubbles using soluble recombinant murine and human Thy1

FACS analysis was performed in order to assess the binding specificity of molecularly-targeted microbubbles to a soluble human and murine Thy1 protein (R&D Systems, USA). To confirm successful ligand conjugation of scFv ligands including His-tag to the microbubble shell, $MB_{Thy1\text{-}scFv}$ was pre-labeled with anti-His antibody-AF488 for 30 minutes at room temperature (Fig. 1D). The microbubbles were washed twice by centrifugation at 300g for 2 min. Subsequently, pre-labeled microbubbles were incubated with 10 nM soluble human and murine IgG-Fc-conjugated Thy1 with 900 μL mouse serum (Sigma-Aldrich, USA) on a benchtop rotator for 40 min at room temperature. This was followed by washing by centrifugation at 300g for 2 min and incubation with anti-human and anti-mouse IgG-Fc antibody-AF647 (eBioscience, USA) for 30 min on ice with a final washing by centrifugation at 300g for 2 min. The measured median fluorescence intensity data was analyzed using FlowJo software. A strong correlation of anti-His antibody-AF488-labeled microbubbles and IgG-Fc antibody-AF647-labeled Thy1 indicated positive binding. All experiments were performed in triplicate.

Cell culture flow chamber cell attachment studies of scFv-conjugated microbubbles

Binding specificity of $MB_{Thy1\text{-}scFv}$ and MB_{Thy1} to the target Thy1 was first assessed in cell culture experiments under flow shear stress conditions simulating flow in blood capillaries by using a flow chamber experimental set-up. Please see Supplementary Methods for more details.

Two mouse models of pancreatic ductal adenocarcinoma (PDAC)

Human Thy1-expressing orthotopic human PDAC xenografts in mice—The Administrative Panel on Laboratory Animal Care of Stanford University approved all procedures using laboratory animals. An orthotopic mouse model expressing human Thy1 on its neovasculature was created as described (6). In brief, human AsPC1 PDAC cells (ATCC, Manassas, VA) were cultured to 70%–80% confluency. After midline laparotomy, the pancreas was exposed, and AsPC1 cells along with $MS1_{Thy1}$ cells at a 1:5 ratio (total of 6×10^6 cells, dissolved in 25 μL Matrigel, BD Biosciences, San Jose, CA) were co-injected into the body or tail of the pancreas in 9 female nude (nu/nu) mice (6–8 weeks old; Charles River, Wilmington, MA). The abdomen was then closed by layers. Orthotopic xenografts were allowed to grow between 7 and 21 days to yield a spectrum of different tumor sizes with diameters ranging between 2.5 and 8.0 mm (mean, 5.1 mm) as measured by B-mode ultrasound.

Transgenic mouse model of PDAC—The transgenic pancreatic cancer mouse model (Pdx1-Cre$^{tg/+}$; KRas$^{LSL\ G12D/+}$; Ink4a/Arf$^{-/-}$) was used (n=6), which spontaneously develops foci of pancreatic cancer within 4–7 weeks after birth (31). Tumor diameters ranged between 1.5 and 4.5 mm (mean, 3.5 mm). Age-matched littermates without KRasG12D mutation were used as normal wild type (WT) control mice (n=6).

Chronic Pancreatitis Model

Chronic pancreatitis was established in 6 transgenic WT mice using two subcutaneous injections of l-arginine dissolved in 0.9% saline (6 g/kg) separated by 1 hour as described (6,32). This was repeated weekly for 6 weeks, after which the mice were allowed to recover for 14 days before imaging experiments.

In vivo ultrasound molecular imaging experiments

All mice were kept anesthetized with 2% isoflurane in room air at 2 L/min on a heated stage for 37°C throughout the ultrasound molecular imaging sessions. In intra-animal comparison experiments, all types of microbubble (5×10^7 each of $MB_{Thy1\text{-}scFv}$, MB_{Thy1}, $MB_{scFv\text{-}scrambled}$, and $MB_{Non\text{-}targeted}$) were injected intravenously through the tail vein of each of the 15 mice (9 nude mice with orthotopic human PDAC xenografts, 6 spontaneous PDAC in transgenic mice) in random order to minimize any bias from injection order. Between imaging sessions using the different contrast agents, a waiting interval of a minimum 30 min was used to allow for clearance of freely circulating microbubbles from the vasculature (3,6). Also, each time at approximately 30 min it was confirmed by imaging that no remaining circulating microbubbles were present from the previous injection and any remaining attached microbubbles were removed by applying a high-power destruction pulse (see below for acoustic parameters). In addition, all control litter mates with normal pancreas (n=6) and all chronic pancreatitis mice (n=6) were scanned as Thy1-negative models after the injection of all four microbubble types. To further confirm binding specificity of $MB_{Thy1\text{-}scFv}$, an *in vivo* competition experiment was performed. In a subgroup of four orthotopic human PDAC-bearing mice, *in vivo* blocking of Thy1 by injecting 150μg Thy-scFv via the tail vein was performed in order to block binding of $MB_{Thy1\text{-}scFv}$ to its target human Thy1.

All *in vivo* imaging studies were performed in contrast mode using a dedicated small-animal high resolution ultrasound imaging system (Vevo 2100; VisualSonics, Canada). Contrast mode images were acquired with a 21-MHz linear transducer (MS250, VisualSonics; lateral and axial resolution of 165 μm and 75 μm, respectively), and all imaging parameters (focal length, 10 mm; transmit power, 4%; mechanical index, 0.2; dynamic range, 40 dB and a center frequency of 21MHz) were kept constant during all imaging sessions. The transducer was fixed on a railing system to maintain the acoustic focus at the center of the PDAC with the imaging plane aligned in the center of the tumor and including adjacent non-PDAC tissue of pancreata. To differentiate the acoustic signal owing to microbubbles adherent to Thy1 and the signal from freely circulating microbubbles in the bloodstream previously described principles of destruction-replenishment techniques were used (6). In brief, the imaging signal in the field of view increases after intravenous injection of molecularly-targeted microbubbles and is composed of signal from attached and freely circulating

microbubbles as well as tissue background signal. After 4 minutes following tail vein injection of microbubbles, 200 frames were acquired. This was followed by a high pressure destructive pulse (1-second continuous high-power destructive pulse of 3.7 MPa, transmit power, 100%; mechanical index, 0.63) to destroy all bound and unbound microbubbles within the beam elevation. After ten seconds to allow freely circulation microbubbles to replenish into the field of view, an additional set of 200 frames was acquired to measure the signal intensity from the unbound circulating microbubbles. The difference in imaging signal pre- and post-destruction was calculated corresponding to the signal from attached microbubbles. The same imaging setting was used in all imaging sessions (Fig. 1E).

Ultrasound molecular imaging data analysis

All imaging data was analyzed by one reader in random order who was blinded to microbubble types. The acoustic imaging signals were analyzed post image acquisition, averaged to compensate for breathing motion artifacts by using commercially available analysis software (VevoCQ; VisualSonics). Data analysis was accomplished by selecting a frame with the plane of interest and manually drawing a region of interest (ROI) around the PDAC in bearing pancreas, in the adjacent non-PDAC pancreatic tissue, as well as in the normal pancreas of control litter mates. The magnitude of imaging signal (expressed in arbitrary units, a.u.) from attached microbubbles was assessed by calculating an average for pre- and post-destruction imaging signals and subtracting the average post-destruction signal from the average pre-destruction signal using Vevo2100 built-in software (VevoCQ; VisualSonics).

Ex vivo analysis of Thy1 expression

Ex vivo analysis was performed using standard techniques (see Supplementary Methods).

Statistical Analysis

All data were expressed as mean ± SD. For details on the statistical analysis, please refer to Supplementary Methods.

Results

Engineering, screening and production of Thy1-scFv ligand

To obtain a human Thy1-scFv ligand, a naïve scFv-yeast library with a diversity of 2.5×10^9 was screened. After seven rounds of iterations, selections and affinity maturations, the final isolated yeast clones showed higher affinity for Thy1 than those obtained from the original yeast library (Fig. 2A). The dominant clone was identified by sequence analysis (Fig. 2B). The 259-amino acid Thy1-binding scFv ligand was produced with an N-terminal 6xHis-tag and an enterokinase-cleavage site fragment. Thy1-scFv was then purified by using a His-Trap FPLC. The molecular weight of Thy1-scFv (44 kDa) was verified by using SDS-PAGE, showing high ligand purity of more than 95% (Fig. 3A).

Characterization and target-specificity of Thy1-scFv

FACS analysis was performed to analyze binding specificity of purified Thy1-scFv to a soluble human and murine Thy1 protein. In comparison to negative control beads, fluorescently-labeled Thy1-scFv showed enhanced fluorescence intensity signal, indicating solely binding to both human and murine Thy1-coated beads (Fig. 3B). The K_D of Thy1-scFv as assessed by FACS was 3.4 ± 0.36 nM for human and 9.2 ± 1.7 nM for murine Thy1 (Fig. 3C). Thy1-scFv also showed binding to Thy1-expressing cells, whereas there was no binding to both Thy1-negative cells (MS1-WT) and CD276-expressing control cells. Furthermore, blocking of Thy1 receptors with free Thy1-scFv resulted in significantly (P<0.01) decreased binding of fluorescently-labeled Thy1-scFv, confirming binding specificity of Thy1-scFv to cellularly Thy1-expressing cells (Fig. 3D). This was further shown by immunofluorescence microscopy (Fig. 3E).

In vitro binding study of $MB_{Thy1\text{-}scFv}$ using FACS

FACS analysis was performed to analyze binding specificity of $MB_{Thy1\text{-}scFv}$ to a soluble human and murine Thy1 protein. Before FACS studies, all microbubbles were fluorescently pre-labeled by anti-His antibody-AF488 and were incubated with human and murine Thy1 protein (Fig. 3F and G). In comparison to non-scFv coated microbubbles (MB_{Thy1} and $MB_{Non\text{-}targeted}$), only His-tagged scFv ligands conjugated to the surface of microbubbles ($MB_{Thy1\text{-}scFv}$ and $MB_{scFv\text{-}scrambled}$) showed enhanced fluorescence intensity signal using anti-His antibody-AF488, indicating successful conjugation of scFv ligands to the surface of microbubbles (Fig. 3F and G). To proof binding specificity of $MB_{Thy1\text{-}scFv}$ to both soluble human and murine Thy1 protein, a binding complex analysis between anti-His antibody-AF488 pre-labeled $MB_{Thy1\text{-}scFv}$ and AF647 post-labeled soluble human and murine Thy1 was performed; it showed a significant (P<0.01) and strong positive correlation (human Thy1, R^2=0.97 ± 0.03; murine Thy1, R^2=0.95 ± 0.02), whereas $MB_{scFv\text{-}scrambled}$ (R^2=0.19 ± 0.02; R^2=0.14 ± 0.01, respectively), and $MB_{Non\text{-}targeted}$ (R^2=0.05 ± 0.04; R^2=0.03 ± 0.0.05, respectively) showed no correlation, indicating no binding to soluble AF647-labeled Thy1 (Fig. 3F and G). A binding complex between pre-labeled Thy1 and MB_{Thy1} (no His-tag) serving as positive control depicted an enhanced AF647 fluorescence intensity signal (Fig. 3F and G). These results confirmed that $MB_{Thy1\text{-}scFv}$ bind specifically to both soluble human and murine Thy1 protein.

Flow chamber cell attachment studies

FACS analysis confirmed overexpression of human Thy1 on $MS1_{Thy1}$ cells, whereas MS1 WT cells did not express Thy1 (Fig. 4A). In flow chamber cell attachment studies simulating flow shear stress conditions in blood capillaries the average number of $MB_{Thy1\text{-}scFv}$ (3.0 ± 0.81 MB/cell) and MB_{Thy1} (3.29 ± 0.75 MB/cell) attached per $MS1_{Thy1}$ cell were significantly higher (P<0.01) than $MB_{scFv\text{-}scrambled}$ (0.57 ± 0.53 MB/cell) (Fig. 4B). Blocking of Thy1 receptors with free Thy1-scFv resulted in significantly (P< 0.01) decreased $MB_{Thy1\text{-}scFv}$ attachment (1.14 ± 0.6 MB/cell), confirming binding specificity of $MB_{Thy1\text{-}scFv}$ to Thy1-expressing MS1 cells. There was significantly lower (P < 0.01) attachment of $MB_{Non\text{-}targeted}$ (0.43 ± 0.53 MB/cell) to Thy1-expressing MS1 cells compared

with both $MB_{Thy1\text{-}scFv}$ and MB_{Thy1}. Overall results suggested that $MB_{Thy1\text{-}scFv}$ binds specifically to human Thy1-expressing cells under flow shear stress conditions (Fig. 4C).

In vivo ultrasound molecular imaging in mouse models of PDAC

To validate binding of $MB_{Thy1\text{-}scFv}$ to both human and murine Thy1 *in vivo*, both an orthotopic human PDAC xenograft expressing human Thy1 on its vasculature as well as a transgenic mouse model of spontaneous PDAC expressing murine Thy1 on its neovasculature were used. *In vivo* ultrasound molecular imaging of orthotopic human PDAC xenografts showed significantly higher imaging signal following $MB_{Thy1\text{-}scFv}$ ($P < 0.01$) and MB_{Thy1} ($P < 0.01$) administration compared to control $MB_{Non\text{-}targeted}$ (Fig. 5A and B). The imaging signals following administration of $MB_{Thy1\text{-}scFv}$ (5.32 ± 1.59 a.u.) and MB_{Thy1} (5.56 ± 1.57 a.u.) were not significantly different ($P = 0.76$). Following injection of control $MB_{scFv\text{-}scrambled}$ (0.9 ± 0.63 a.u.), imaging signal was significantly ($P < 0.01$) lower compared to the signal after $MB_{Thy1\text{-}scFv}$ and not significantly different ($P = 0.65$) compared to $MB_{Non\text{-}targeted}$ (0.78 ± 0.48 a.u.) (Fig. 5A and B). Furthermore, imaging signal was significantly lower ($P < 0.01$) in adjacent normal pancreas tissue after injection of all microbubbles types ($MB_{Thy1\text{-}scFv}$, 0.41 ± 0.23 a.u.; MB_{Thy1}, 0.38 ± 0.24 a.u.; $MB_{scFv\text{-}scrambled}$, 0.17 ± 0.2 a.u.; $MB_{Non\text{-}targeted}$, 0.3 ± 0.22 a.u.) (Fig. 5A). To further confirm Thy1-binding specificity of $MB_{Thy1\text{-}scFv}$ in orthotopic human PDAC xenografts, *in vivo* blocking of Thy1 receptors with free Thy1-scFv was performed and resulted in a significant decrease of Thy1-targeted imaging signal by 55.81% ($P < 0.05$, 2.38 ± 0.81 a.u.) compared to tumors without pre-administration of the blocking agent (Fig. 5C and D).

Similarly, in spontaneous murine PDAC of transgenic mice, imaging signal was significantly higher following $MB_{Thy1\text{-}scFv}$ ($P < 0.01$) and MB_{Thy1} ($P < 0.01$) administration compared to $MB_{Non\text{-}targeted}$ (Fig. 6A and B). Furthermore, the imaging signals following administration of $MB_{Thy1\text{-}scFv}$ (5.68 ± 2.5 a.u.) and following MB_{Thy1} (5.85 ± 2.1 a.u.) were not significantly different ($P = 0.9$). Also, following injection of $MB_{scFv\text{-}scrambled}$ (1.21 ± 0.93 a.u.), imaging signal was significantly ($P < 0.01$) lower compared to the signal using $MB_{Thy1\text{-}scFv}$ and not significantly different ($P = 0.54$) compared to $MB_{Non\text{-}targeted}$ (0.92 ± 0.73 a.u.). Furthermore, for all microbubbles types imaging signal was significantly lower ($P < 0.01$) in adjacent pancreas tissue of transgenic mice ($MB_{Thy1\text{-}scFv}$, 0.51 ± 0.3 a.u.; MB_{Thy1}, 0.47 ± 0.32 a.u.; $MB_{scFv\text{-}scrambled}$, 0.34 ± 0.26 a.u.; $MB_{Non\text{-}targeted}$, 0.26 ± 0.23 a.u.) (Fig. 6A).

Also, as a negative control for non-angiogenic Thy1-negative vessels, normal pancreata in wild type mice were scanned after intravenous administration of $MB_{Thy1\text{-}scFv}$, MB_{Thy1}, $MB_{scFv\text{-}scrambled}$, and $MB_{Non\text{-}targeted}$ (Fig. 6C). Imaging signal in normal pancreata was significantly lower ($P < 0.01$; $MB_{Thy1\text{-}scFv}$, 0.67 ± 0.71 a.u.; MB_{Thy1}, 0.68 ± 0.29 a.u.; $MB_{scFv\text{-}scrambled}$, 0.32 ± 0.2 a.u.; $MB_{Non\text{-}targeted}$ 0.21 ± 0.1 a.u.) for all microbubble types compared to PDAC (Fig. 6C).

Finally, all microbubble types were further tested in a chronic pancreatitis model as a model of benign disease and additional negative control. Imaging signal was also significantly lower ($P < 0.01$) in chronic pancreatitis tissues compared to PDAC for all microbubbles

types ($MB_{Thy1\text{-}scFv}$, 0.84 ± 0.6 a.u.; MB_{Thy1}, 0.71 ± 0.73 a.u.; $MB_{scFv\text{-}scrambled}$, 0.48 ± 0.28 a.u.; $MB_{Non\text{-}targeted}$, 0.26 ± 0.18 a.u.).

Ex vivo immunofluorescence analysis

Histological analysis of tissue H&E-stained slices confirmed presence of PDAC in orthotopic human xenografts and transgenic mice (Fig. 6D and E). Similar to *in vivo* ultrasound imaging results, fluorescence imaging showed accumulation of fluorescently labeled $MB_{Thy1\text{-}scFv}$ within the neovasculature of PDAC in both orthotopic human xenografts and spontaneous PDAC in transgenic mice (Fig. 6F and G). Furthermore, *ex vivo* immunofluorescence analysis confirmed overexpression of human Thy1 on the neovasculature of orthotopic human PDAC xenografts and of murine Thy1 on the neovasculature of PDAC in transgenic mice. Quantitative immunofluorescence showed significantly ($P < 0.01$) increased co-localization of human (0.46 ± 0.09 a.u.) and murine (0.51± 0.08 a.u.; green) Thy1 on CD31-stained (red) tumor vessels compared to normal pancreata (0.10 ± 0.07 a.u.) and chronic pancreatitis tissues (0.13 ± 0.06 a.u.) (Fig. 6H).

Discussion

This study exemplifies the proof-of-principle approach from engineering a human Thy1-scFv ligand binding to both human and murine Thy1 to *in vitro*, cell culture, and *in vivo* validation of Thy1-targeted microbubbles for ultrasound molecular imaging of PDAC in two animal models, a human PDAC xenograft and a transgenic mouse model.

Ultrasound is a promising imaging technique for early cancer detection due to its inherent advantages compared to other imaging approaches, including wide availability, portability, relatively low cost, lack of ionizing radiation exposure, deep tissue penetration, and high spatial resolution (33,34). Combined with endoscopy, ultrasound of the pancreas can also be performed in patients with limited acoustic windows. Adding contrast microbubbles that are molecularly-targeted at molecules expressed in PDAC can substantially increase the ability of ultrasound to detect and characterize small foci of cancer (35). In this proof-of-principle study we engineered a novel human Thy1-scFv ligand and tested whether it could be used for ultrasound molecular imaging of PDAC. Several antibodies from nonhuman species targeting Thy1 are commercially available that can be used for molecular imaging of PDAC. However, antibodies from nonhuman species are immunogenic and can cause severe allergic reactions in patients (36,37); therefore, these ligands can only be used for preclinical imaging. While many humanized antibodies have been successfully created and used in patients, the development and production of full-length antibodies against a specific target is challenging, costly, and time-consuming (38). Therefore, there is a critical need for an alternative platform to allow engineering of biocompatible, target specific, and high affinity binding ligands that are smaller, less expensive, and faster to produce than conventional full-length antibodies (39). Antibody-like molecules with exposed loops or surfaces that can be randomized, modified, and screened using selective phage or yeast engineered libraries are promising alternative platforms to engineer ligands that bind to molecular imaging targeted with high affinity and specificity (16). Several types of engineered binding ligands have been explored for ultrasound molecular imaging including knottins (40), nanobodies (41),

fibronectins (42), and peptides (43). Engineered scFvs are an alternative platform for designing binding ligands for molecular imaging with several advantages (16,44). Since scFv are smaller than full-length antibodies owing to the lack of an Fc fragment, the risk for immunogenicity is minimized (45). Also, recombinant scFvs can be produced cost efficiently. Furthermore, scFvs are versatile and can be modified by adding site-specific tags for detection and bioconjugation (46). Finally, scFv have already shown good safety profile in phase I and II clinical trials in patients (19,47).

In this study, we have used a naïve nonimmune human scFv-yeast surface display library for engineering and screening of scFv binding to human and murine Thy1. Our results showed that the engineered human Thy1-scFv ligand from a human yeast surface display library not only binds to soluble human and murine Thy1 as well as to Thy1 expressed on live cells, but that it can also be used to functionalize contrast microbubbles for ultrasound imaging PDAC *in vivo*. For testing *in vivo* binding to murine Thy1, a well-established transgenic mouse model was used that resembles spontaneous development of PDAC in patients (31). This animal model has been previously shown to overexpress murine Thy1 on its neovasculature (6,48), which was confirmed by quantitative immunofluorescence in our current study. For testing *in vivo* binding to human Thy1, we used a previously described orthotopic human PDAC xenograft model (6) which expresses human Thy1 on its neovasculature by co-injecting human PDAC cells with vascular endothelial cells expressing human Thy1. These human Thy1-expressing cells are integrated into the neovasculature of the xenografts during angiogenesis and tumor growth, thereby allowing microbubbles to be tested for binding to human Thy1 in a mouse model before moving into clinical trials.

We acknowledge the following limitation of our study. For this proof of concept study, biotin/streptavidin coupling was used for conjugating engineered Thy1-scFv onto microbubbles. While this is a well-established approach for preclinical testing of new contrast microbubbles due to its flexible, quick, and site-specific conjugation chemistry, these types of microbubbles are not useful for clinical translation due to the immunogenicity of streptavidin (36). Efforts are under way to develop site-specific modifications on Thy1-scFv to enable alternative bioconjugation of the ligands to the microbubble shell for eventual clinical translation. Also, while transgenic mice may develop multiple tumor foci in the pancreas, we imaged only one focus of PDAC in this study to evaluate imaging signals obtained from different types of microbubbles in an intra-animal comparison study without assessing the whole pancreas for additional foci of cancer. Also, due to the limited number of imaged tumors, imaging signal was not stratified by tumor size. Future prospective studies are warranted to assess the minimally detectable tumor size along with sensitivity and specificity of Thy1-targeted contrast microbubbles for ultrasound molecular imaging of PDAC.

In conclusion, our results suggest that a novel Thy1-scFv ligand can be engineered for improved detection of PDAC using ultrasound molecular imaging. Ongoing developments are aimed at designing a next generation clinically translatable Thy1-targeted contrast microbubble.

Supplementary Material

Refer to Web version on PubMed Central for supplementary material.

Acknowledgments

Financial support:

This research was supported by the NIH R01CA155289 grant, the NIH R21EB022770, the R41CA203090, NIH U01CA210020, and by the Canary Foundation. The Mildred-Scheel Cancer Foundation from Germany provided funding for Dr. Lotfi Abou-Elkacem to study abroad at Stanford University.

We would like to acknowledge the SCi^3 Core imaging facilities and the Canary Center at Stanford for the technical support of this study.

References

1. Siegel RL, Miller KD, Jemal A. Cancer Statistics, 2017. CA Cancer J Clin. 2017; 67:7–30. [PubMed: 28055103]
2. Rahib L, Smith BD, Aizenberg R, Rosenzweig AB, Fleshman JM, Matrisian LM. Projecting cancer incidence and deaths to 2030: the unexpected burden of thyroid, liver, and pancreas cancers in the United States. Cancer Res. 2014; 74:2913–21. [PubMed: 24840647]
3. Shaib YH, Davila JA, El-Serag HB. The epidemiology of pancreatic cancer in the United States: changes below the surface. Aliment Pharmacol Ther. 2006; 24:87–94. [PubMed: 16803606]
4. Cid-Arregui A, Juarez V. Perspectives in the treatment of pancreatic adenocarcinoma. World J Gastroenterol. 2015; 21:9297–316. [PubMed: 26309356]
5. Liang JJ, Kimchi ET, Staveley-O'Carroll KF, Tan D. Diagnostic and prognostic biomarkers in pancreatic carcinoma. Int J Clin Exp Pathol. 2009; 2:1–10. [PubMed: 18830385]
6. Foygel K, Wang H, Machtaler S, Lutz AM, Chen R, Pysz M, et al. Detection of pancreatic ductal adenocarcinoma in mice by ultrasound imaging of thymocyte differentiation antigen 1. Gastroenterology. 2013; 145:885–94. e3. [PubMed: 23791701]
7. Gessner R, Dayton PA. Advances in molecular imaging with ultrasound. Mol Imaging. 2010; 9:117–27. [PubMed: 20487678]
8. Pysz MA, Willmann JK. Targeted contrast-enhanced ultrasound: an emerging technology in abdominal and pelvic imaging. Gastroenterology. 2011; 140:785–90. [PubMed: 21255573]
9. Zhu J, Thakolwiboon S, Liu X, Zhang M, Lubman DM. Overexpression of CD90 (Thy-1) in pancreatic adenocarcinoma present in the tumor microenvironment. PLoS One. 2014; 9:e115507. [PubMed: 25536077]
10. Tse AG, Barclay AN, Watts A, Williams AF. A glycophospholipid tail at the carboxyl terminus of the Thy-1 glycoprotein of neurons and thymocytes. Science. 1985; 230:1003–8. [PubMed: 2865810]
11. Reif AE, Allen JM. The Akr Thymic Antigen and Its Distribution in Leukemias and Nervous Tissues. J Exp Med. 1964; 120:413–33. [PubMed: 14207060]
12. St Croix B, Rago C, Velculescu V, Traverso G, Romans KE, Montgomery E, et al. Genes expressed in human tumor endothelium. Science. 2000; 289:1197–202. [PubMed: 10947988]
13. Madden SL, Cook BP, Nacht M, Weber WD, Callahan MR, Jiang Y, et al. Vascular gene expression in nonneoplastic and malignant brain. Am J Pathol. 2004; 165:601–8. [PubMed: 15277233]
14. Chen X, Higgins J, Cheung ST, Li R, Mason V, Montgomery K, et al. Novel endothelial cell markers in hepatocellular carcinoma. Mod Pathol. 2004; 17:1198–210. [PubMed: 15154008]
15. Bradley JE, Ramirez G, Hagood JS. Roles and regulation of Thy-1, a context-dependent modulator of cell phenotype. Biofactors. 2009; 35:258–65. [PubMed: 19422052]
16. Chao G, Lau WL, Hackel BJ, Sazinsky SL, Lippow SM, Wittrup KD. Isolating and engineering human antibodies using yeast surface display. Nat Protoc. 2006; 1:755–68. [PubMed: 17406305]

17. Adams GP, Schier R. Generating improved single-chain Fv molecules for tumor targeting. J Immunol Methods. 1999; 231:249–60. [PubMed: 10648942]
18. Bao X, Chandramohan V, Reynolds RP, Norton JN, Wetsel WC, Rodriguiz RM, et al. Preclinical toxicity evaluation of a novel immunotoxin, D2C7-(scdsFv)-PE38KDEL, administered via intracerebral convection-enhanced delivery in rats. Invest New Drugs. 2016; 34:149–58. [PubMed: 26728879]
19. Bachanova V, Frankel AE, Cao Q, Lewis D, Grzywacz B, Verneris MR, et al. Phase I study of a bispecific ligand-directed toxin targeting CD22 and CD19 (DT2219) for refractory B-cell malignancies. Clin Cancer Res. 2015; 21:1267–72. [PubMed: 25770294]
20. Posey JA, Khazaeli MB, Bookman MA, Nowrouzi A, Grizzle WE, Thornton J, et al. A phase I trial of the single-chain immunotoxin SGN-10 (BR96 sFv-PE40) in patients with advanced solid tumors. Clin Cancer Res. 2002; 8:3092–9. [PubMed: 12374676]
21. Pavlinkova G, Colcher D, Booth BJ, Goel A, Wittel UA, Batra SK. Effects of humanization and gene shuffling on immunogenicity and antigen binding of anti-TAG-72 single-chain Fvs. Int J Cancer. 2001; 94:717–26. [PubMed: 11745468]
22. Holliger P, Hudson PJ. Engineered antibody fragments and the rise of single domains. Nat Biotechnol. 2005; 23:1126–36. [PubMed: 16151406]
23. Wei LH, Olafsen T, Radu C, Hildebrandt IJ, McCoy MR, Phelps ME, et al. Engineered antibody fragments with infinite affinity as reporter genes for PET imaging. J Nucl Med. 2008; 49:1828–35. [PubMed: 18927335]
24. Bradbury AM, Pluckthun A. Antibodies: validate recombinants once. Nature. 2015; 520:295.
25. Bradbury A, Pluckthun A. Reproducibility: Standardize antibodies used in research. Nature. 2015; 518:27–9. [PubMed: 25652980]
26. Mazzucchelli S, Verderio P, Sommaruga S, Colombo M, Salvade A, Corsi F, et al. Multiple presentation of Scfv800E6 on silica nanospheres enhances targeting efficiency toward HER-2 receptor in breast cancer cells. Bioconjug Chem. 2011; 22:2296–303. [PubMed: 22010849]
27. Seki T, Spurr N, Obata F, Goyert S, Goodfellow P, Silver J. The human Thy-1 gene: structure and chromosomal location. Proc Natl Acad Sci U S A. 1985; 82:6657–61. [PubMed: 2864690]
28. Kimura RH, Teed R, Hackel BJ, Pysz MA, Chuang CZ, Sathirachinda A, Willmann JK, et al. Pharmacokinetically stabilized cystine knot peptides that bind alpha-v-beta-6 integrin with single-digit nanomolar affinities for detection of pancreatic cancer. 2012
29. Kimura RH, Levin AM, Cochran FV, Cochran JR. Engineered cystine knot peptides that bind alphavbeta3, alphavbeta5, and alpha5beta1 integrins with low-nanomolar affinity. Proteins. 2009; 77:359–69. [PubMed: 19452550]
30. Lipovsek D, Lippow SM, Hackel BJ, Gregson MW, Cheng P, Kapila A, et al. Evolution of an interloop disulfide bond in high-affinity antibody mimics based on fibronectin type III domain and selected by yeast surface display: molecular convergence with single-domain camelid and shark antibodies. J Mol Biol. 2007; 368:1024–41. [PubMed: 17382960]
31. Aguirre AJ, Bardeesy N, Sinha M, Lopez L, Tuveson DA, Horner J, et al. Activated Kras and Ink4a/Arf deficiency cooperate to produce metastatic pancreatic ductal adenocarcinoma. Genes Dev. 2003; 17:3112–26. [PubMed: 14681207]
32. Otsuki M, Yamamoto M, Yamaguchi T. Animal models of chronic pancreatitis. Gastroenterol Res Pract. 2010; 2010:403295. [PubMed: 21197438]
33. Willmann JKBL, Testa A, Rinaldi P, Rindi G, Valluru KS, Petrone G, Martini M, Lutz AM, Gambhir SS. Ultrasound molecular imaging in patients with breast and ovarian lesions: first-in-human results. 2016 (in review).
34. Willmann JK, van Bruggen N, Dinkelborg LM, Gambhir SS. Molecular imaging in drug development. Nat Rev Drug Discov. 2008; 7:591–607. [PubMed: 18591980]
35. Laeseke PF, Chen R, Jeffrey RB, Brentnall TA, Willmann JK. Combining in Vitro Diagnostics with in Vivo Imaging for Earlier Detection of Pancreatic Ductal Adenocarcinoma: Challenges and Solutions. Radiology. 2015; 277:644–61. [PubMed: 26599925]
36. Marshall D, Pedley RB, Boden JA, Boden R, Melton RG, Begent RH. Polyethylene glycol modification of a galactosylated streptavidin clearing agent: effects on immunogenicity and

clearance of a biotinylated anti-tumour antibody. Br J Cancer. 1996; 73:565–72. [PubMed: 8605088]

37. Meyer DL, Schultz J, Lin Y, Henry A, Sanderson J, Jackson JM, et al. Reduced antibody response to streptavidin through site-directed mutagenesis. Protein Science. 2001; 10:491–503. [PubMed: 11344318]
38. Shukla AA, Thommes J. Recent advances in large-scale production of monoclonal antibodies and related proteins. Trends Biotechnol. 2010; 28:253–61. [PubMed: 20304511]
39. Gebauer M, Skerra A. Engineered protein scaffolds as next-generation antibody therapeutics. Curr Opin Chem Biol. 2009; 13:245–55. [PubMed: 19501012]
40. Willmann JK, Kimura RH, Deshpande N, Lutz AM, Cochran JR, Gambhir SS. Targeted contrast-enhanced ultrasound imaging of tumor angiogenesis with contrast microbubbles conjugated to integrin-binding knottin peptides. J Nucl Med. 2010; 51:433–40. [PubMed: 20150258]
41. Hernot S, Unnikrishnan S, Du Z, Shevchenko T, Cosyns B, Broisat A, et al. Nanobody-coupled microbubbles as novel molecular tracer. J Control Release. 2012; 158:346–53. [PubMed: 22197777]
42. Abou-Elkacem L, Wilson KE, Johnson SM, Chowdhury SM, Bachawal S, Hackel BJ, et al. Ultrasound Molecular Imaging of the Breast Cancer Neovasculature using Engineered Fibronectin Scaffold Ligands: A Novel Class of Targeted Contrast Ultrasound Agent. Theranostics. 2016; 6:1740–52. [PubMed: 27570547]
43. Pysz MA, Foygel K, Rosenberg J, Gambhir SS, Schneider M, Willmann JK. Antiangiogenic cancer therapy: monitoring with molecular US and a clinically translatable contrast agent (BR55). Radiology. 2010; 256:519–27. [PubMed: 20515975]
44. Yao VJ, D'Angelo S, Butler KS, Theron C, Smith TL, Marchio S, et al. Ligand-targeted theranostic nanomedicines against cancer. J Control Release. 2016; 240:267–86. [PubMed: 26772878]
45. Santos AD, Kashmiri SV, Hand PH, Schlom J, Padlan EA. Generation and characterization of a single gene-encoded single-chain-tetravalent antitumor antibody. Clin Cancer Res. 1999; 5:3118s–23s. [PubMed: 10541352]
46. Massa S, Xavier C, Muyldermans S, Devoogdt N. Emerging site-specific bioconjugation strategies for radioimmunotracer development. Expert Opin Drug Deliv. 2016; 13:1149–63. [PubMed: 27116898]
47. Topp MS, Kufer P, Gokbuget N, Goebeler M, Klinger M, Neumann S, et al. Targeted therapy with the T-cell-engaging antibody blinatumomab of chemotherapy-refractory minimal residual disease in B-lineage acute lymphoblastic leukemia patients results in high response rate and prolonged leukemia-free survival. J Clin Oncol. 2011; 29:2493–8. [PubMed: 21576633]
48. Gordon JW, Chesa PG, Nishimura H, Rettig WJ, Maccari JE, Endo T, et al. Regulation of Thy-1 gene expression in transgenic mice. Cell. 1987; 50:445–52. [PubMed: 2886226]

Translational Relevance

Pancreatic ductal adenocarcinoma (PDAC) is a highly lethal cancer. Most patients are diagnosed at advanced stage with poor outcomes. The thymocyte differentiation antigen 1 (Thy1) has been previously identified and validated as a promising molecular marker differentially expressed on the neovasculature of human PDAC compared to chronic pancreatitis and normal pancreas. The current study was directed towards the development and assessment of a clinically translatable dual human and murine Thy1-binding single-chain-antibody ligand (Thy1-scFv) for contrast microbubble-enhanced ultrasound molecular imaging of PDAC. *In vivo* ultrasound molecular imaging using Thy1-scFv conjugated to microbubbles demonstrated specific-binding to Thy1 and imaging signals were substantially higher in both orthotopic human PDAC xenografts and transgenic PDAC compared to chronic pancreatitis and normal pancreas tissue. Ongoing translational studies are targeted at developing clinical grade Thy1-targeted microbubbles which may improve visualization of PDAC and enable diagnosing at earlier disease state to ultimately improve survival of PDAC patients.

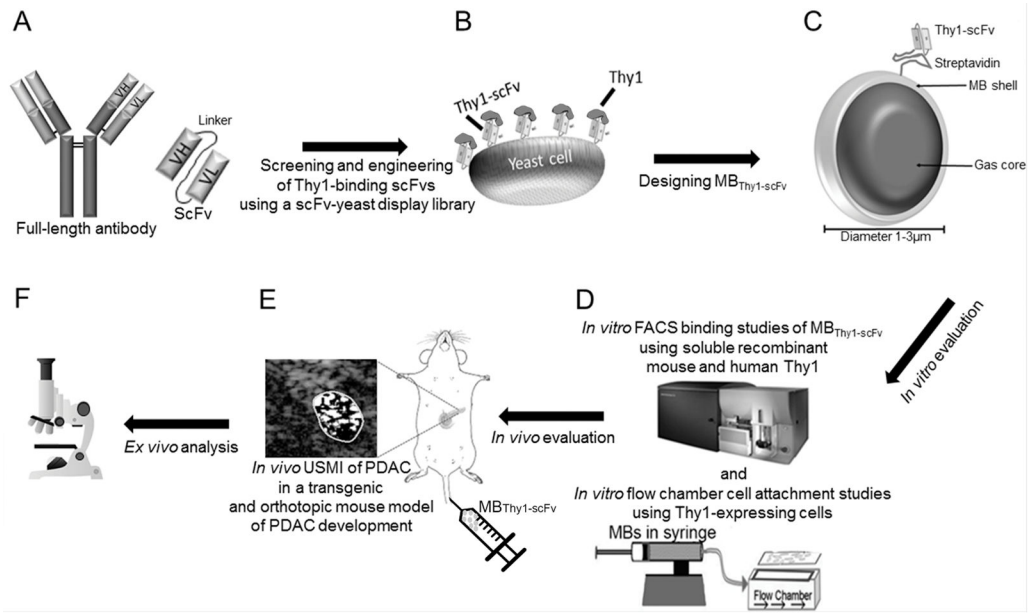

Figure 1.

Schematic drawing of overall study design. **A,** shows a single-chain Fv fragment (scFv) compared to a full-length antibody. **B,** Thy1-scFv ligand to both human and murine Thy1 was engineered using a naïve nonimmune human scFv-yeast surface display library. **C,** Thy1-targeted contrast microbubbles ($MB_{Thy1\text{-}scFv}$) were generated by attaching biotinylated Thy1-scFv on the surface of streptavidin-containing microbubbles. **D,** $MB_{Thy1\text{-}scFv}$ were tested for Thy1 binding both *in vitro* and on live cells in flow chamber experiments, as well as **E,** *in vivo* in two mouse models. **F,** Thy1 expression on the neovasculature of both mouse models was confirmed by *ex vivo* quantitative immunofluorescence.

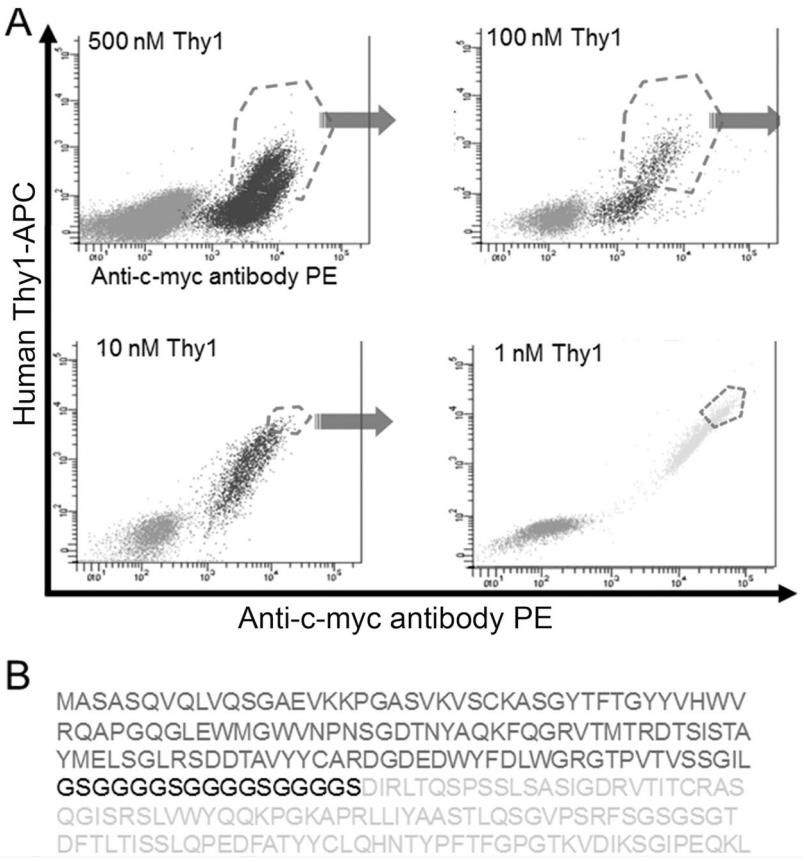

Figure 2.

Screening of Thy1-binding scFv in a naïve nonimmune human scFv yeast surface display library. **A,** FACS profiles of the original naïve human scFv yeast surface display library (left) using 500nM Thy1 protein. After seven rounds of iterations, selections and affinity maturations, the final isolated yeast clones showed higher affinity for Thy1 than those obtained from the original yeast library (500nM) and sub-clones after initial error-prone polymerase chain reaction (100nM, 10nM). A dominant clone (1nM, right panel) with high binding affinity to human Thy1 was identified and sorted by FACS. **B,** Amino acid sequence of the isolated Thy1-scFv. The engineered Thy1-scFv consists of variable regions of heavy (N-terminal) and light (C-terminal) chains, which are joined together by a flexible peptide linker (black).

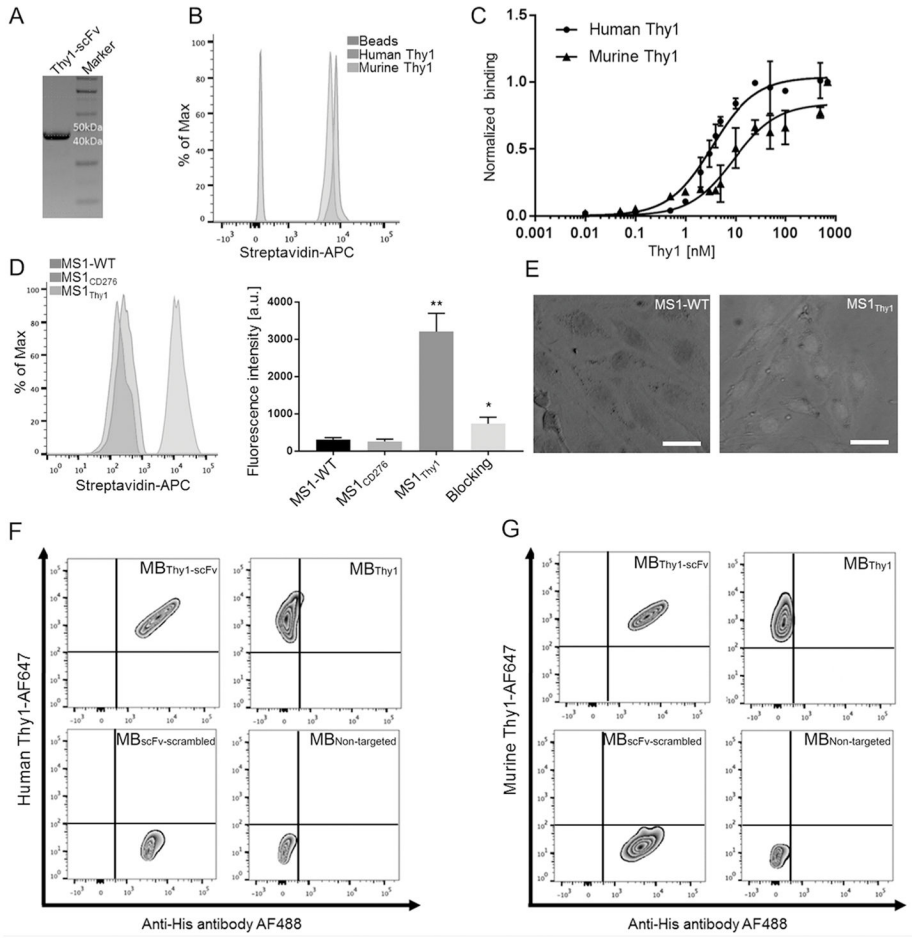

Figure 3.

Purification and characterization of Thy1-scFv. **A,** His-Trap FPLC-purified Thy1-scFv (MW 44kDa) was analyzed by SDS-PAGE under reducing conditions followed by Coomassie blue staining. **B,** Binding of Thy1-scFv to human and murine Thy1-coated beads. As a negative control, naked streptavidin-beads and beads coated with biotinylated human IgG (beads, left) were used. Note, only Thy1-scFv bound to human and murine Thy1-coated beads (human and murine Thy1, right). **C,** Affinity measurement of Thy1-scFv to human Thy1 protein using FACS showing a K_D of 3.4 ± 0.36 nM (human Thy1) and 9.2 ± 1.7 nM (murine Thy1). Data were normalized with respect to saturated fluorescence intensity (plateau) observed at the highest target concentrations. **D,** Measurement of Thy1-scFv binding to cells using FACS. Thy1-scFv showed binding to $MS1_{Thy1}$, whereas no binding to Thy1-negative cells (MS1-WT and $MS1_{CD276}$) cells could be detected. Thy1-expression on MS1 cells was confirmed with significantly increased fluorescence intensity (**, $P < 0.01$) compared to Thy1-negative cells and significant decreased fluorescence after blocking the receptors (*, $P < 0.01$). **E,** Representative fluorescence microscopy images of cells stained with Thy1-scFv ($MS1_{Thy1}$, right), further confirming specific binding of Thy1-scFv ligand to $MS1_{Thy1}$ cells. Cell nuclei were stained with 4′,6-diamidino-2-phenylindole (DAPI). Scale bar = 20 μm. All results are representatives of at least three independent experiments. **F, G,** *In vitro* binding specificity study of $MB_{Thy1\text{-}scFv}$. Binding specificity of $MB_{Thy1\text{-}scFv}$ and MB_{Thy1} with

fluorescent soluble human (**F**) and murine (**G**) Thy1 was analyzed using FACS. $MB_{Thy1\text{-}scFv}$ and $MB_{scFv\text{-}scrambled}$ showed an enhanced geometric mean fluorescence intensity which indicates the presence of an anti-His-AF488-antibody binding to scFv-coated microbubbles. A clear correlation between $MB_{Thy1\text{-}scFv}$ to the soluble AF647-labeled Thy1 demonstrated a specific binding of Thy1-scFv. As a positive control, MB_{Thy1} showed enhanced geometric mean fluorescence intensity towards AF647-labeled Thy1 (**A and B**). As a negative control, $MB_{scFv\text{-}scrambled}$ and $MB_{Non\text{-}targeted}$ showed no binding to human (**A**) and murine (**B**) Thy1. The cut-off (quad gate bar) was defined based on the background geometric mean fluorescence intensity of $MB_{Non\text{-}targeted}$ and $MB_{scFv\text{-}scrambled}$.

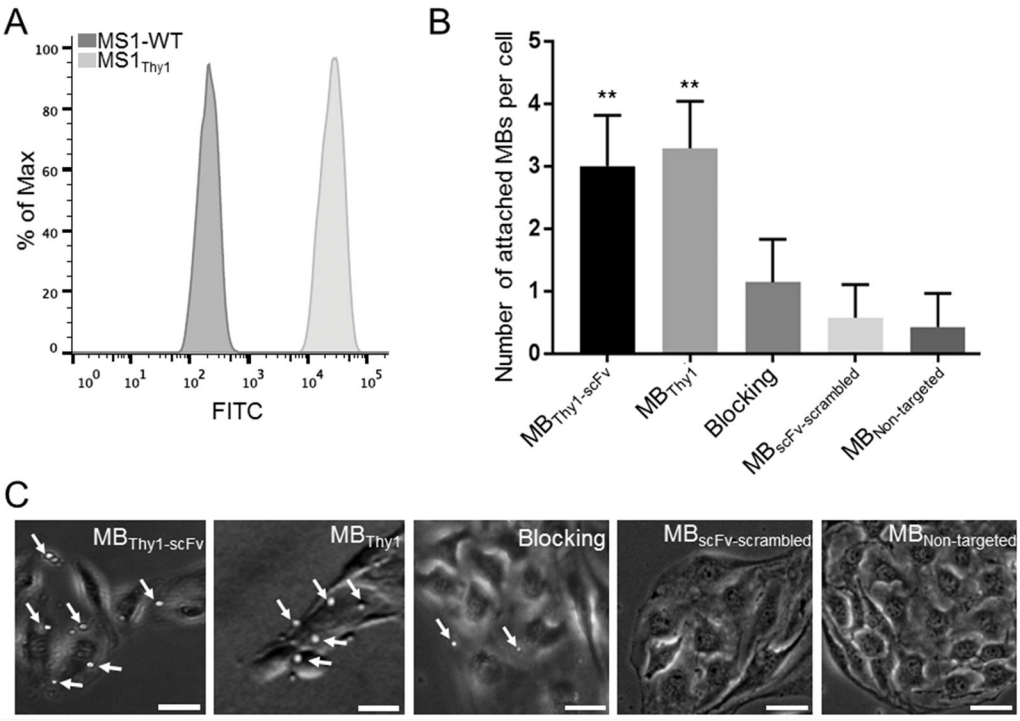

Figure 4.

Flow chamber cell attachment studies on live cells using four types of microbubbles (MBs). **A,** Thy1 overexpression on $MS1_{Thy1}$ compared to MS1-WT cells was confirmed by FACS. **B**, Bar graph summarizes quantitative flow chamber cell culture data using the four types of contrast microbubbles as well as results after blocking Thy1. Error bar = standard deviation; **, $P < 0.01$ compared to control conditions. **C,** Representative photomicrographs from flow chamber cell culture experiments with Thy1-expressing MS1 cells exposed to $MB_{Thy1\text{-}scFv}$, MB_{Thy1}, $MB_{scFv\text{-}scrambled}$, and $MB_{Non\text{-}targeted}$ along with blocking experiments confirm binding of $MB_{Thy1\text{-}scFv}$ and positive control MB_{Thy1} to Thy1 under flow shear stress conditions. Microbubbles (arrows) are visualized as white spherical dots. Scale bar = 10 μm.

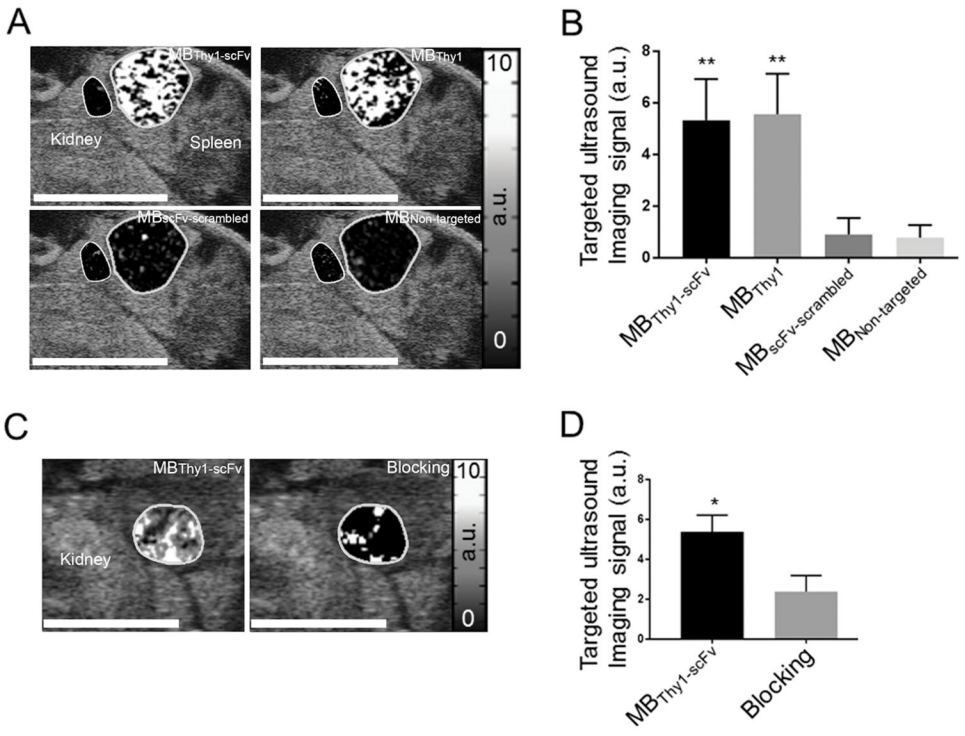

Figure 5.

In vivo ultrasound molecular imaging in orthotopic human PDAC xenograft tumor model in mice. **A,** Representative transverse contrast mode ultrasound images overlaid on B-mode images show strong signal in PDAC (region of interest, right) after injection of both $MB_{Thy1\text{-}scFv}$ and positive control MB_{Thy1}, but only background signal following injection of the two negative control microbubbles ($MB_{scFv\text{-}scrambled}$ and $MB_{Non\text{-}targeted}$). Only background signal was noted in adjacent normal pancreas after injection of all microbubble types (left region of interest was drawn to quantify imaging signal in adjacent non-PDAC pancreatic tissue). Note, spleen and kidney are marked on B-mode images for anatomical guidance. **B,** Bar graph summarizes quantitative *in vivo* imaging data using the various types of contrast microbubbles. Error bar = standard deviation; **, $P < 0.01$. **C, D,** Representative *in vivo* ultrasound imaging examples of an orthotopic human PDAC xenograft scanned before and after intravenous administration of free blocking Thy1-scFv. Scale bar = 5 mm; color coded scale is shown for ultrasound molecular imaging signal in arbitrary units (a.u.). **D**, Bar graph summarizes quantitative results from *in vivo* blocking experiments. Error bar = standard deviation; *, $P < 0.05$.

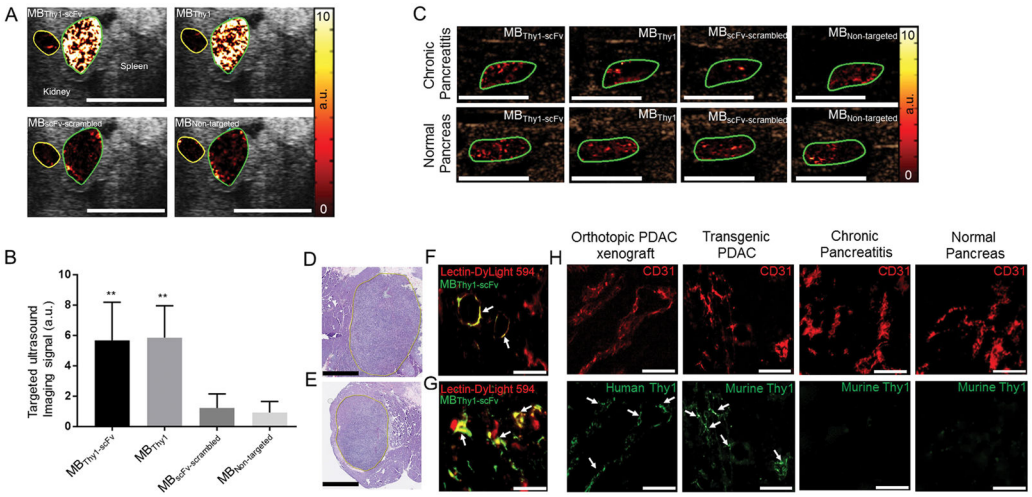

Figure 6.

In vivo ultrasound molecular imaging of PDAC in transgenic mice, a chronic pancreatitis model, and in normal pancreas tissues. **A,** Representative transverse contrast mode ultrasound images overlaid on B-mode images show strong signal in PDAC (green region of interest) after injection of $MB_{Thy1\text{-}scFv}$ and MB_{Thy1}, but only background signal following injection of the two types of control microbubbles ($MB_{scFv\text{-}scrambled}$ and $MB_{Non\text{-}targeted}$). Only background signal was noted in adjacent normal pancreas after injection of all microbubble types (a yellow region of interest was drawn to quantify imaging signal in adjacent non-PDAC pancreatic tissue). **B,** Bar graph summarizes quantitative *in vivo* imaging data sets using the various types of contrast microbubbles. Error bar = standard deviation; **, $P < 0.01$. **C,** Representative transverse contrast mode ultrasound images show only background imaging signal in chronic pancreatitis and normal pancreas tissue after injection of all four types of microbubbles; scale bar = 5 mm; color coded scale is shown for ultrasound molecular imaging in arbitrary units (a.u.). **D and E,** Corresponding hematoxylin-eosin-stained sample (original magnification, ×10) confirms presence of PDAC in orthotopic human xenograft (**D**) and transgenic mouse model (**E**) imaged in Figure 5A and Fig 6A, respectively. Scale bar = 1 mm. **F and G,** Micrographs show accumulation and co-localization (white arrows) of fluorescently labeled $MB_{Thy1\text{-}scFv}$ (green) within the neovasculature (red) of PDAC in orthotopic human xenograft (**F**) and transgenic mouse (**G**). Scale bar = 100 μm. **H,** Representative immunofluorescence staining micrographs for CD31 and Thy1 in human PDAC xenografts, transgenic PDAC, chronic pancreatitis, and normal pancreas tissue. PDAC showed strong expression of Thy1 on the vasculature (co-localization of Thy1 (green) on CD31-stained (red) tumor vessels) compared to chronic pancreatitis and normal pancreas tissue. Scale bar = 50 μm.